Full-Wave Analysis of an Infinitely Long Magnetic Surface Wave Transducer

EL-BADAWY EL-SHARAWY, MEMBER, IEEE, AND ROBERT W. JACKSON, SENIOR MEMBER, IEEE

Abstract—**This paper presents a rigorous analysis of an infinitely long microstrip line embedded in a multilayer structure which includes a ferrite layer. In certain frequency ranges, such a line launches magnetic surface waves in the ferrite and thus becomes a surface wave transducer. The analysis described herein is a self-consistent full-wave solution which rigorously includes the effect of radiating magnetic waves. By expanding the transducer currents in terms of both even and odd functions, it is shown that the principal current is not symmetrically distributed across the transducer width. The propagation constant of the transducer mode is complex and shows a large imaginary part (attenuation) tied to the excitation of magnetostatic surface waves. In addition, the propagation constant remains complex even for frequencies above the magnetostatic surface wave bandwidth. This has been found to be due to the excitation of magnetic surface waves having complex propagation constants.**

Measurements of the insertion loss of a multilayer microstrip transducer are presented and are in reasonable agreement with the calculated attenuation.

I. Introduction

AN EFFICIENT approach [1] has recently been introduced for the analysis of multilayer ferrite structures. In this technique, Green's functions which relate electric fields and currents are formulated using the transmission matrix of the structure. This paper extends this approach to include the analysis of magnetostatic surface wave (MSSW) transducers.

Theoretical and experimental work on delay line transducers was initially presented by Ganguly and Webb [2]. Further work included edge effects on line currents [3] and the finite width of ferrite films [4]. In previous papers, the magnetostatic approximation has been employed; i.e., retardation effects are ignored. The validity of this approximation has been verified for several simple structures [5]–[9]; however, the accuracy degrades with increasing ferrite film thickness [6] or increasing dc magnetic field [8], and possibly for very strong surface wave coupling [2], [3]. Furthermore, although the radiation of MSSW's is not symmetric in practical transducers [2], previous theories have always assumed the transducer currents to be symmetrically distributed across the transducer width. To date this assumption has not been examined.

This paper employs Galerkin's moment method to solve for the propagation constant of an infinite-length microstrip transducer in a multilayer structure of infinite extent. Retardation effects are included and currents on the microstrip line are expanded in terms of a complete set of even and odd basis functions. The attenuation constant of the line is studied and a peak value is observed at the resonance frequency of the MSSW. The attenuation continues to exist above the resonance and can peak again. This behavior cannot be explained using the available theories, which predict that all types of magnetic surface waves are cut off above the resonance.

To explain such behavior, this paper first examines the dispersion relations for ferrite surface waves including all electromagnetic effects. Various multilayer structures are investigated and the results verified where possible by comparison to the magnetostatic solutions. The analysis calculates the complex propagation constant for a general direction in the plane of the magnetization. In the literature, similar studies have been confined to real surface waves propagating in a single lossless ferrite slab [6]. In addition, the results presented in this paper reveal the existence of a complex type of surface wave which can be excited above the resonance frequency of the MSSW. The propagation constants of such waves are found to be complex for both lossy and lossless materials.

The electromagnetic analysis of magnetic surface waves is described in Section II. Next, the analysis of the infinitely long transducer is described in subsections A and B of Section III. Measurements of attenuation along an MSSW transducer are described in subsection III-C and compared with predictions. The conclusions drawn from this work are presented in Section IV.

II. Electromagnetic Solution for Magnetic Surface Waves

A. Theory

In this section, a dispersion relation is formulated for surface waves which propagate in the geometries shown in Fig. 1. The transmission matrix approach is used to derive the dispersion. In this approach, tangential electric and magnetic fields on one boundary of a ferrite layer are expressed in terms of the fields on the other boundary.

Manuscript received May 22, 1989; revised January 10, 1990.

E. El-Sharawy was with the Department of Electrical and Computer Engineering, University of Massachusetts, Amherst, MA 01003. He is now with the Department of Electrical and Computer Engineering, Arizona State University, Tempe, AZ 85287.

R. W. Jackson is with the Department of Electrical and Computer Engineering, University of Massachusetts, Amherst, MA 01003.

IEEE Log Number 9034917.

0018-9480/90/0600-0730$01.00

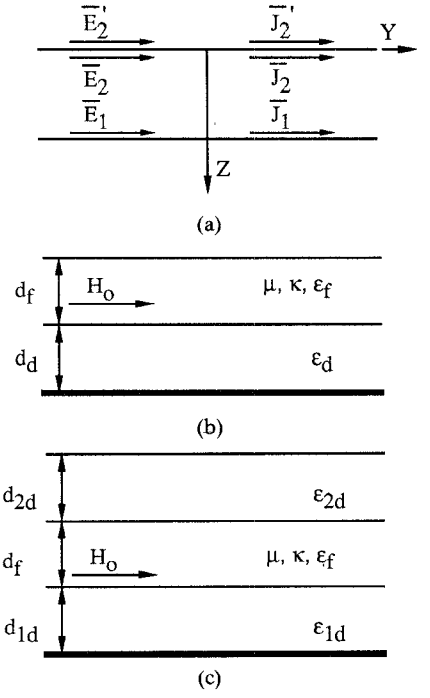

Fig. 1. (a) The generic geometry used in the analysis of multilayer MSSW structures such as (b) a two-layer structure and (c) a three-layer structure.

This is significantly different from the transmission-line-like approach suggested by Itoh in [10] (usually referred to as the spectral-domain immittance approach). In particular, the immittance approach can only be applied to isotropic substrates, where fields can be written as a superposition of TM and TE waves with a well-defined characteristic admittance for each wave. In ferrite substrates, all fields are generally coupled [1], [11], [12] and are neither TE nor TM. In addition, two eigenwaves with two different wavenumbers must be used to describe the ferrite fields [1], [11], [12]. Therefore the characteristic admittance of a ferrite medium is not well defined. The transmission matrix formulation as described here does not require splitting the fields into TE and TM; nor does it include any characteristic admittance of the medium. The transmission formulation will also be used for the analysis in Section III; therefore the following discussion sets the notation for both Section II and Section III.

The surface wave analysis for the three configurations assumes infinite extents in the x and y directions with a field spatial dependence in the form

$$\boldsymbol{E}(x,y,z) = \boldsymbol{E}(z)e^{-j\beta_x x}e^{-j\beta_y y}$$

$$\boldsymbol{H}(x,y,z) = \boldsymbol{H}(z)e^{-j\beta_x x}e^{-j\beta_y y} \tag{1}$$

where β_x and β_y are the propagation constants in the x and y directions, respectively. Splitting $\boldsymbol{E}$ and $\boldsymbol{H}$ into components which are longitudinal and transverse to the magnetization (y direction) and solving Maxwell's equations for the y components results in the following equations:

$$\frac{\partial^2 E_y}{\partial z^2} - \left(\beta_x^2 + \beta_y^2 - \omega^2\epsilon\frac{\mu^2-\kappa^2}{\mu}\right)E_y = j\omega\mu_0\beta_y\frac{\kappa}{\mu}H_y \tag{2a}$$

$$\frac{\partial^2 H_y}{\partial z^2} - \left(\beta_x^2 + \frac{\mu_0}{\mu}\beta_y^2 - \omega^2\mu_0\epsilon\right)H_y = -j\omega\epsilon\beta_y\frac{\kappa}{\mu}E_y \tag{2b}$$

where μ_0, μ, and κ are the elements of the permeability tensor for the ferrite material [13] and ϵ is the ferrite permittivity. Equations (2) can be solved for E_y and H_y [1] and then used to determine the other field components according to

$$E^{\pm} = \frac{j\beta_y\nabla^{\pm}E_y \pm \omega(\mu\pm\kappa)\nabla^{\pm}H_y}{\beta_y^2 - \omega^2\epsilon(\mu\pm\kappa)} \tag{3a}$$

$$H^{\pm} = \frac{j\beta_y\nabla^{\pm}H_y \mp \omega\epsilon\nabla^{\pm}E_y}{\beta_y^2 - \omega^2\epsilon(\mu\pm\kappa)} \tag{3b}$$

where

$$E^{\pm} = E_z \pm jE_x \tag{4a}$$

$$H^{\pm} = H_z \pm jH_x \tag{4b}$$

$$\nabla^{\pm} = \frac{\partial}{\partial z} \pm \beta_x. \tag{4c}$$

Following the procedure described in [1], the fields at the surfaces of a ferrite layer (see Fig. 1(a)) may be related according to

$$\begin{bmatrix}\boldsymbol{E}_2\\ \boldsymbol{J}_2\end{bmatrix} = \bar{\bar{T}}\begin{bmatrix}\boldsymbol{E}_1\\ \boldsymbol{J}_1\end{bmatrix} = \begin{bmatrix}\bar{\bar{T}}_E & \bar{\bar{Z}}_T\\ \bar{\bar{Y}}_T & \bar{\bar{T}}_J\end{bmatrix}\begin{bmatrix}\boldsymbol{E}_1\\ \boldsymbol{J}_1\end{bmatrix} \tag{5}$$

where $\boldsymbol{E}_1$ and $\boldsymbol{E}_2$ are the tangential electric fields at surfaces 1 and 2. $\boldsymbol{J}_1$ and $\boldsymbol{J}_2$ are the surface currents defined by $\boldsymbol{J}_i = \hat{z}_i \times \boldsymbol{H}_i$, where $\boldsymbol{H}_i$ is the tangential magnetic field at the ith surface just inside the slab being considered (Fig. 1(a)). $\bar{\bar{T}}_E, \bar{\bar{Z}}_T, \bar{\bar{Y}}_T$, and $\bar{\bar{T}}_J$ are 2×2 submatrices of the transmission matrix $\boldsymbol{T}$ given in [1]. We note that the transmission matrix of a multilayer structure can be formed by simply multiplying the transmission matrices of the individual layers in the correct sequence.

In most applications it is desirable to find the relation between $\boldsymbol{J}$ and $\boldsymbol{E}$ at a particular surface under various circumstances. Suppose, for example, we wish to relate $\boldsymbol{J}_2$ and $\boldsymbol{E}_2$ with the diadic, $\bar{\bar{G}}_s$. If a conducting plane is located on surface 1, then $\boldsymbol{E}_1 = 0$ and (5) can be reduced to

$$\boldsymbol{J}_2 = \bar{\bar{G}}_s\boldsymbol{E}_2 = \bar{\bar{T}}_J\bar{\bar{Z}}_T^{-1}\boldsymbol{E}_2. \tag{6}$$

On the other hand, if a semi-infinite half-space is present below surface 1, then $\bar{\bar{G}}_s$ can be expressed as [1]

$$\bar{\bar{G}}_s = \left(\bar{\bar{Y}}_T + \bar{\bar{T}}_J\bar{\bar{G}}_1\right)\left(\bar{\bar{T}}_E + \bar{\bar{Z}}_T\bar{\bar{G}}_1\right)^{-1} \tag{7}$$

where $\bar{\bar{G}}_1$ is listed in the Appendix and relates $\boldsymbol{J}_1$ to $\boldsymbol{E}_1$ as

$$\boldsymbol{J}_1 = \bar{\bar{G}}_1\boldsymbol{E}. \tag{8}$$

The same procedure used to find $\boldsymbol{J}_2$ in terms of $\boldsymbol{E}_2$ in (6)

and (7) can be used to find the current due to fields in the upper region above surface 2. This relation is given by

$$\boldsymbol{J}_2' = \overline{\overline{G}}_s' \boldsymbol{E}_2 \tag{9}$$

where $\boldsymbol{J}_2' = -\hat{z} \times \boldsymbol{H}_2'$ and prime denotes the fields, currents, and relating function $\overline{\overline{G}}_s'$. In the special case of a semi-infinite upper space, $\overline{\overline{G}}_s'$ becomes exactly the same as $\overline{\overline{G}}_1$ of (8). The total surface current $\boldsymbol{J}_s$ on surface 2 can be expressed in terms of $\boldsymbol{J}_2'$ and $\boldsymbol{J}_2$ as

$$\boldsymbol{J}_s = \hat{z} \times (\boldsymbol{H}_2 - \boldsymbol{H}_2') = \boldsymbol{J}_2 + \boldsymbol{J}_2' = \left(\overline{\overline{G}}_s + \overline{\overline{G}}_s'\right)\boldsymbol{E}_2. \tag{10}$$

The continuity of the tangential electric field is implicit in (9) and (10), whereas the continuity of the magnetic fields can be imposed by forcing $\boldsymbol{J}_s = 0$. This can only happen for nonzero $\boldsymbol{E}_2$ if β_x and β_y are chosen such that

$$|\overline{\overline{G}}_s + \overline{\overline{G}}_s'| = 0. \tag{11}$$

The determinant of the 2×2 matrix in (11) is the surface wave dispersion relation, and the resulting values of β_x and β_y form the mode solution for a wave propagating at an angle ϕ with respect to the direction of magnetization (y axis) such that

$$\phi = \tan^{-1}\frac{\mathrm{Re}(\beta_x)}{\mathrm{Re}(\beta_y)}. \tag{12}$$

In the common case of a single ferrite slab, (11) reduces to

$$\left|\left(\overline{\overline{Y}}_T + \overline{\overline{T}}_J\overline{\overline{G}}_1\right) + \overline{\overline{G}}_1\left(\overline{\overline{T}}_E + \overline{\overline{Z}}_T\overline{\overline{G}}_1\right)\right| = 0. \tag{13}$$

Solutions obtained from (13) for the MSSW dispersion in a single ferrite slab have been verified by comparison to those calculated using the available theories in the literature [6], [8]. The agreement with both references was found to be within 3% for low values of $H_0 (H_0 \leqslant 4\pi M_s)$, where H_0 is the impressed dc magnetic field and $4\pi M_s$ is the magnetization. The discrepancy with [8] rose to about 5% for higher values of $H_0 (H_0 > 4\pi M_s)$. In the next section, further verification and comparison to results based on the magnetostatic approach will be discussed.

The computational efficiency of this approach is an improvement with respect to the approach described in [6], where an 8×8 matrix must be forced to zero in order to find the dispersion for a single ferrite slab. For a large number of layers, the order of the matrix in [6] increases whereas the method presented in this work always results in a 2×2 matrix, regardless of the number of slabs. Lastly, we note that formulating dispersion equation (11) at or near the surface where the surface wave fields are likely to be concentrated results in the best numerical accuracy. This is presumed to be due to the fact that MSSW fields propagate on a specific surface and rapidly decay away from the plane of this surface [14].

Expression (11) could also be used to study the dispersion of forward and backward volume waves. However, since volume waves are cut off over the MSSW bandwidth

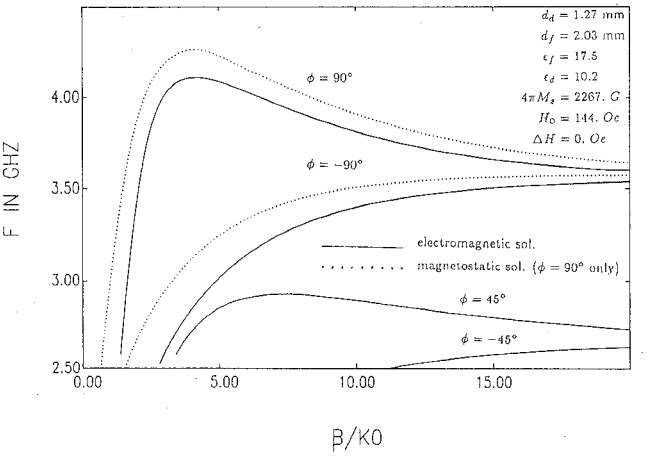

Fig. 2. Dispersion of MSSW in multilayer structure in Fig. 1(b) calculated using magnetostatic and electromagnetic analyses.

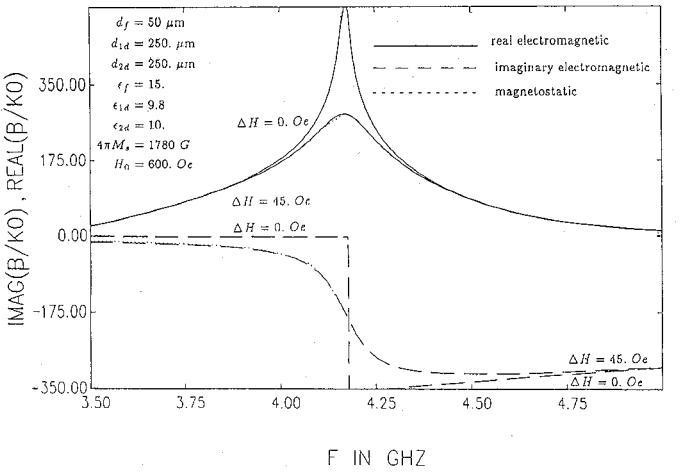

Fig. 3. Complex propagation constant of MSSW in multilayer structure in Fig. 1(c). Note that f_r = 4.17 GHz.

[14], they are not of concern in this paper and their numerical behavior has not been studied thoroughly.

B. Results

The dispersion diagram of MSSW-like modes, calculated using the aforementioned approach, is shown in Fig. 2 for the structure depicted in Fig. 1(b). Losses are neglected and the ferrite layer thickness is chosen to be comparable to the dielectric thickness to enhance the nonreciprocal behavior [15]. This figure shows also the possible discrepancy between magnetostatic and electromagnetic solutions, especially for low values of the propagation constant. Also, the bandwidth of MSSW for a multilayer structure decreases as the direction of propagation gets closer to the direction of magnetization. This is also observed in single ferrite films [14].

The effect of magnetic losses can be included by taking into account the line width, ΔH, of the ferrite material [13]. Fig. 3 shows the complex dispersion diagram for the structure shown in Fig. 1(c), with the direction of propagation being perpendicular to the direction of magnetization. This figure shows the electromagnetic and magneto-

static solutions for both lossy and lossless YIG films. In contrast to the previous figure, the discrepancy in this figure between the magnetostatic and electromagnetic solutions is small. This is because the thickness of the ferrite film in Fig. 3 is 50 μm, compared to 2.03 mm in Fig. 2. As the thickness of the YIG film decreases, larger values of the propagation constant are predicted [6], [14], [15] and the discrepancy between the two different approaches starts to disappear [6].

From Fig. 3 we note that the major difference between the lossy and lossless ferrite layers is the absence of the dispersion singularity at the resonance, ω_r, given by [14], [15]

$$\omega_r = \omega_0 + \frac{\omega_m}{2} \tag{14}$$

where $\omega_0 = \gamma H_0$, $\omega_m = 4\pi\gamma M_s$, and γ is the gyromagnetic ratio. Above this resonance, a sharp increase occurs in the imaginary part of the propagation constant and a sharp decrease occurs in the real part. There is no magnetostatic solution over this range of frequencies for comparison.

In general, a complex propagation constant can result from radiative power leakage from the surface, material losses, or field evanescence along the path of propagation. The first of these was found to be negligible by adding another ground plane to the structure shown in Fig. 1(b) at a distance of 1.0 cm above the ferrite layer so as to reflect any radiated power. Only minor changes in the propagation constant were observed for both lossless and lossy cases. In this respect, the new complex waves are different from the leaky surface waves described in [16]. For frequencies above ω_r, Im(β) increases with decreasing line width and thus material losses alone cannot explain the existence of the complex propagation constant. We conclude that the surface wave roots are complex irrespective of loss or, in other words, are partially evanescent. In the general case where the ferrite line width takes a finite value ($\Delta H \neq 0$), both losses and wave evanescence may be used to explain the imaginary part of the propagation constant. Both the lossy and lossless modes described in Fig. 3 become cut off (propagation constants are purely imaginary) just above 5 GHz.

III. Full-Wave Solution for MSSW Transducers

A. Theory

This subsection describes the formulation used to compute the complex propagation constant, β, of a microstrip line (infinitely long MSSW transducer) in the excitation geometries shown in Fig. 4. When operating at frequencies below and near the magnetostatic surface wave resonance, ω_r, the microstrip line radiates MSSW's and thus becomes a MSSW transducer.

The solution assumes an infinitely long microstrip oriented along the y axis. To find the Green's function for such a formulation, we start by assuming the fields in the

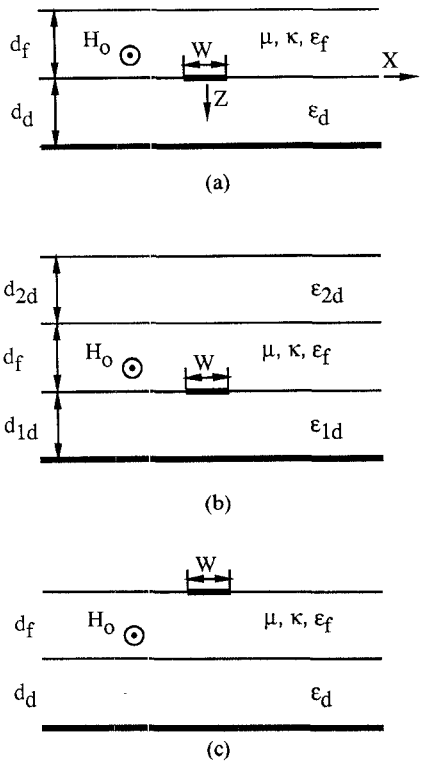

Fig. 4. Geometry of MSSW transducers in multilayer structures.

form

$$\boldsymbol{E} = \boldsymbol{E}(x,z)e^{-j\beta y} \tag{15a}$$

$$\boldsymbol{J} = \boldsymbol{J}(x,z)e^{-j\beta y}. \tag{15b}$$

Following this assumption, a Fourier transform in the x direction is performed. The Green's function can then be determined by using the transmission matrix formulation described previously. The required Green's function in this case relates the tangential electric fields and currents $\boldsymbol{E}_s$ and $\boldsymbol{J}_s$ at the surface containing the microstrip according to the integral relation

$$\begin{aligned}\boldsymbol{E}_s &= \frac{1}{2\pi}\int_{-\infty}^{\infty} \overline{\overline{G}}\cdot\tilde{\boldsymbol{J}}_s e^{jk_x x}\,dk_x \\ &= \frac{1}{2\pi}\int_{-\infty}^{\infty}\left(\overline{\overline{G}}_s + \overline{\overline{G}}_s'\right)^{-1}\cdot\tilde{\boldsymbol{J}}_s e^{jk_x x}\,dk_x\end{aligned} \tag{16}$$

where the tilde ($\sim$) denotes the Fourier transform with respect to x. $\overline{\overline{G}}_s$ and $\overline{\overline{G}}_s'$ have been defined previously. The electric currents on the microstrip line are then expanded according to

$$\begin{aligned}J_y(x) &= \sum_{n=0}^{N_y} c_n f_{yn} \\ J_x(x) &= \sum_{n=0}^{N_x} d_n f_{xn}\end{aligned} \tag{17}$$

where

$$f_{yn} = (-1)^n T_n\left(\frac{2x}{W}\right) \Bigg/ \sqrt{1-\left(\frac{2x}{W}\right)^2}, \qquad |x| < W/2 \tag{18a}$$

$$f_{xn} = (-1)^n U_n\left(\frac{2x}{W}\right) \sqrt{1-\left(\frac{2x}{W}\right)^2}, \qquad |x| < W/2 \tag{18b}$$

and both functions are zero for $|x| > W/2$. W is the width of the microstrip line, and (T_n, U_n) are Chebyshev polynomials of the first and second kinds. Both even and odd values of n will be used to account for the current asymmetry caused by surface wave nonreciprocity. This will be discussed later in more detail.

The final step in the moment method formulation is to test $\boldsymbol{E}_s$ with the same basis function as given by (18). The resulting impedance matrix, $\overline{\overline{Z}}$, can be expressed as

$$\overline{\overline{Z}} = \begin{bmatrix} \overline{\overline{Z}}_{xx} & \overline{\overline{Z}}_{xy} \\ \overline{\overline{Z}}_{yx} & \overline{\overline{Z}}_{yy} \end{bmatrix} \tag{19}$$

and

$$Z_{mn}^{pq} = \int_{-\infty}^{\infty} F_{pm}^{*}(k_x) G_{pq}(k_x, -\beta) F_{qn}(k_x)\, dk_x \tag{20}$$

where F is the Fourier transform of the basis functions in (18):

$$F_{yn} = j^n \frac{\pi W}{2} J_n\left(\frac{k_x W}{2}\right) \tag{21a}$$

$$F_{xn} = j^n \frac{\pi W}{2} (n+1) J_{n+1}\left(\frac{k_x W}{2}\right) \Bigg/ \frac{k_x W}{2}. \tag{21b}$$

Integral (20) is evaluated numerically and β is varied until a solution which forces the determinant of $\overline{\overline{Z}}$ to zero is found.

For lossless ferrite, the excitation of surface waves will introduce poles on the real k_x axis. In addition, branch points and branch cuts [17] can further complicate the evaluation of (20). In this case a complex contour integral similar to that discussed in [17] and [18] is required to enclose the surface wave poles and avoid crossing branch cuts. The effect of finite ferrite losses is to move the poles and branch points off the real axis, making a straightforward numerical integration of (20) possible. However, low values of loss still require a careful adjustment of parameters, such as the resolution of the numerical integration, the integral limits, and the number of basis functions.

B. Results

Before presenting the results, the convergence of the solutions will be discussed. First, the integration resolution and the integral limits are chosen such that a variation of less than $\pm 0.5\%$ in Z_{mn}^{pq} is observed from any further (but finite) increase in the resolution or the limits. Second, the number of transverse current basis functions, N_x, is chosen to be equal to 1 less than the number of the longitudinal current basis function, N_y; therefore the total number of basis functions N_β will equal $2N_y - 1$. Choosing $N_x = N_y - 1$ is the usual choice for microstrip lines since the lowest order transverse current is of the same magnitude as the second-order longitudinal current. Therefore, the convergence of the solution for the propagation constant will be tested by varying N_β.

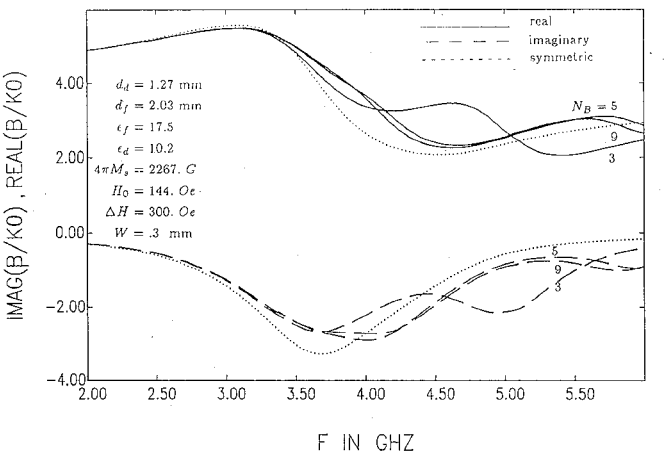

Fig. 5. Convergence of the normalized propagation constant of the MSSW transducer in Fig. 4(a).

The real and imaginary parts of the computed propagation constant are shown in Fig. 5 for the geometry shown in Fig. 4(a). Note that the MSSW for this geometry is shown in Fig. 2. The number of basis functions in Fig. 5 was varied from $N_\beta = 1$ to $N_\beta = 9$.

The simple case of $N_\beta = 1$ represents the case of an even symmetric current J_y on the microstrip line ($N_y = 1$, $N_x = 0$). It has been found that, for small values of the width ($W < 0.1\lambda_0$), increasing the number of basis functions while keeping the even symmetry of J_y and the odd symmetry of J_x will give almost the same results as using a single symmetric mode.

The other solutions in Fig. 5, $N_\beta = 3$, $N_\beta = 5$, and $N_\beta = 9$, include both even and odd basis functions in the expansion of J_x and J_y and thus the possibility of a current asymmetry is allowed. The convergence in this case may be slow, but will give more accurate results than the symmetric current solution. For example, the figure shows that the asymmetric current solution predicts a peak attenuation constant of $2.731k_0$ at 4.05 GHz. Assuming a symmetric current distribution results in a peak attenuation of $3.289k_0$ at 3.67 GHz. The discrepancy between the two solutions is due to a current asymmetry on the line. Fig. 6 shows the longitudinal currents for the structure analyzed in Fig. 5 using the two different assumptions. In the asymmetric current solution, the imaginary part of the current switches signs on opposite edges. This shows the existence of certain types of eddy currents on the line. Also, the real part of the current is higher at one edge than the other. The current asymmetry on the line is due to the nonreciprocal properties of MSSW. These are: (a) oppositely propagating surface waves ($+x$ and $-x$ directions) have different dispersion characteristics as shown in Fig. 2; and (b) the amplitude maxima of

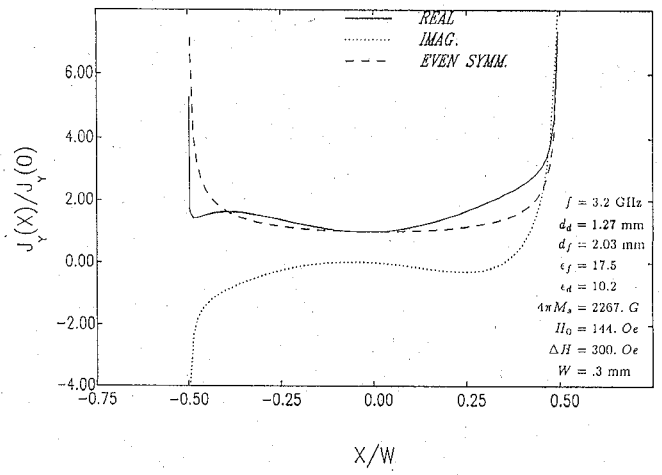

Fig. 6. Current on a microstrip transducer in structure in Fig. 4(a) compared to the symmetric current which is usually assumed.

these oppositely propagating surface waves occur on opposite sides of the ferrite films [2]. Both properties will result in different excitation conditions at the two edges of the line, causing the line current to be asymmetric.

Often the simplified analysis of microstrip transducers assumes a real propagation constant, which is calculated by assuming that the ferrite layer is replaced by a dielectric layer with the same permittivity [2]. For the configuration analyzed in Fig. 5, such a calculation results in a propagation constant of roughly $3.52k_0$ and this remains fairly constant ($\pm 0.3\%$) over the band of frequencies shown in the figure. This approximate value is significantly different from the rigorous results shown.

The attenuation and the real part of the propagation constant of a practical microstrip transducer (the structure in Fig. 4(b)) are plotted in, respectively, parts (a) and (b) of Fig. 7. This figure shows both the symmetric and the asymmetric solution; the attenuation has two peaks of 22.5 dB/cm at 4.18 GHz and 36.7 dB/cm at 4.61 GHz. The first peak corresponds to the MSSW resonance $\omega_r =$ 4.17 GHz. Below ω_r, surface waves propagate in the ferrite layer with relatively low losses and leak from the microstrip. Higher attenuation over this band means better coupling to the MSSW. The rigorous calculation of the real part of the propagation constant, plotted in Fig. 7(b), should be compared to the values obtained via the conventional approximation, $3.28k_0$ (constant over the band). Significant differences are evident.

Above ω_r it is necessary to consider the possible reasons for the nonzero imaginary part of the microstrip propagation constant. Inserting or removing a (distant) cover plate has no effect on the computed propagation constant; thus space wave radiation is not a factor. Fig. 3 shows that the magnetic surface waves above ω_r are partially evanescent (complex propagation constant) with or without loss. Therefore no energy is radiated away via these waves. The only other source of energy loss might be material loss, but decreasing the material loss (the line width) actually increases the imagainary part of the microstrip propagation constant. Thus material losses are not the only source of propagation constant complexity.

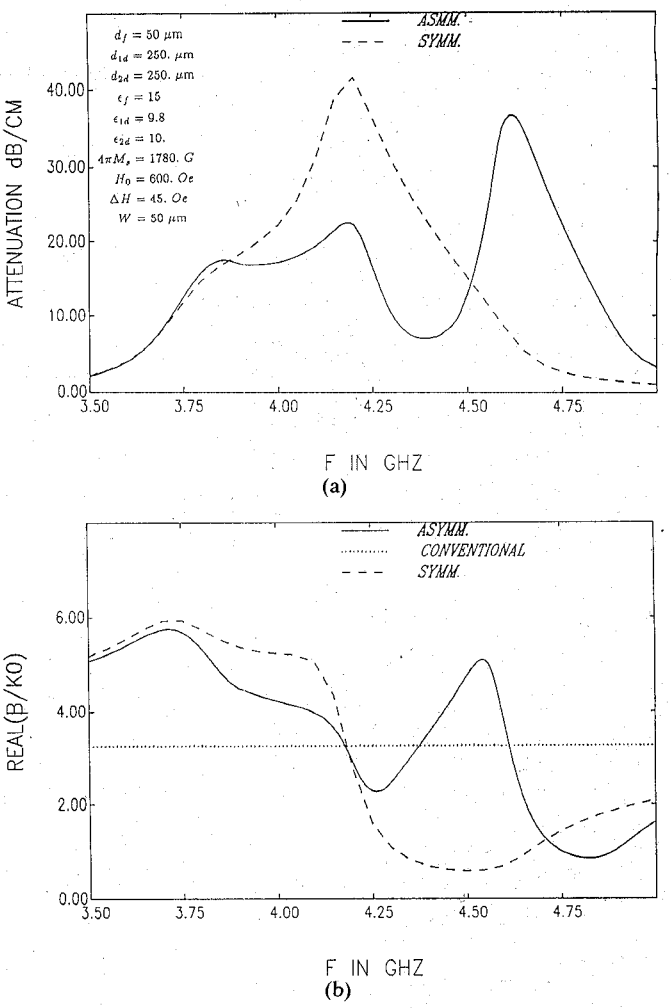

Fig. 7. (a) Attenuation and (b) propagation constant for a mode traveling on a practical MSSW transducer: ---- symmetry assumed; —— symmetry not assumed; ···· conventional assumption where ferrite is replaced with dielectric.

Since the aforementioned sources of energy loss do not entirely explain the complex propagation constant, we conclude that the microstrip solutions on ferrite, at frequencies just above ω_r, are partially evanescent in the same way as the solutions found in [19] for enclosed microstrip on a dielectric slab. In that work, complex propagation constants were found to occur for some higher order modes even when no source of loss was present. Furthermore, a comparison of Figs. 3 and 7 shows that the peak in the imaginary part of the microstrip propagation constant occurs very near the frequency where the imaginary part of the surface wave peaks (4.52 GHz and 4.61 GHz, respectively). It therefore seems likely that the partial evanescence of the microstrip mode is due to an interaction with the partially evanescent surface wave mode.

The current symmetry assumption used in previous theories [2]–[4] will result only in one predicted attenuation peak of 41.5 dB/cm at 4.18 GHz for the structure under consideration. Also, with this assumption, the calculated attenuation and propagation constants over the MSSW band are generally higher than those in the solution with some asymmetry allowed.

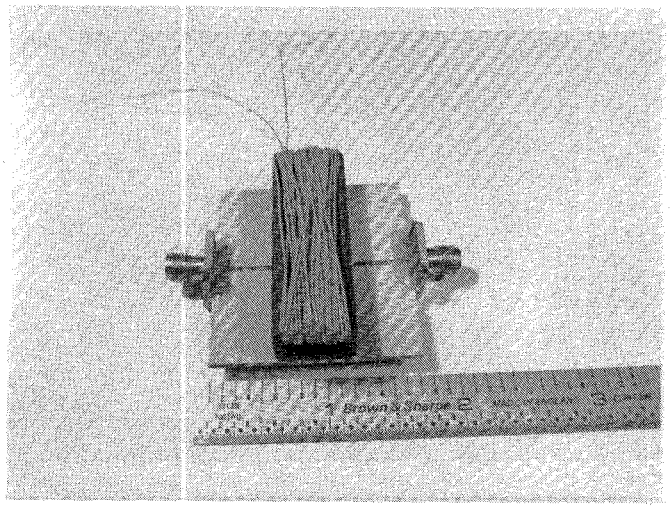

Fig. 8. Experimental structure for measurement of mode attenuation on a MSSW transducer.

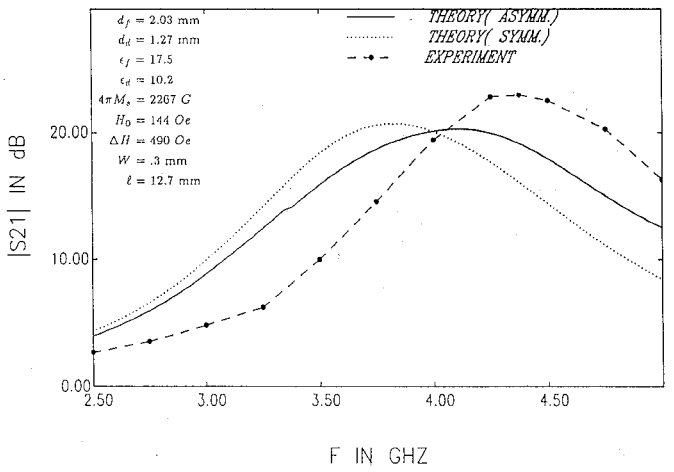

Fig. 9. Theory and measurement of the mode attenuation along a MSSW transducer.

C. Experimental Verification

In this subsection, measurements of the insertion loss of a multilayer microstrip MSSW transducer are described and compared with analysis. The microstrip line was etched on 0.050-in.-thick RT Duroid 6010.2, which has a dielectric constant of 10.2. The line was 300 μm wide and 12.7 mm long and was tapered to a 50 Ω impedance in order to allow a good coax–microstrip transition. A rectangular ferrite toroid was placed on top of the line to complete the ferrite–dielectric structure. The outer dimensions of the toroid were $15.24 \times 10.16 \times 44.45$ mm^3 and the wall thickness was 2.03 mm. The corners on the outer sides were chamfered by 0.9 mm to ensure the alignment between the magnetization and the RF fields [20]. The toroid was magnetized by a wire wound around the top horizontal wall as shown in Fig. 8. The current passed through this wire resulted in an H_0 of about 144 Oe. The ferrite material has a measured magnetization of 2267 G $\pm$ 10% and a 3 dB line width (ΔH) of 490 Oe $\pm$ 2% at 9 GHz. The line width measurement is, however, somewhat sensitive to surface conditions [21], [22] and to operating frequency [23].

The insertion loss, plotted in Fig. 9, was measured using the HP 8510 network analyzer. The measured return loss was about 15 dB or more between 2.5 and 3.5 GHz. Above 3.5 GHz the return loss starts to increase and has a peak value of 8 dB at 4.3 GHz; it then starts decreasing again. Note that when two successive toroids were used on a line identical to that described above, the measured insertion loss doubles and the return loss remains almost the same. Therefore, below ω_r (3.58 GHz) the insertion loss effects shown in Fig. 9 are assumed to be due solely to MSSW and ferrite material loss. Above ω_r ferrite material loss dominates over any possible evanescent mode effects. The structure shown in Fig. 4(a) was used to model the experimental structure. The MSSW's and the convergence of the propagation constant of this structure were described in Figs. 2 and 5, respectively. The calculated attenuation is also shown in Fig. 9 for comparison. For $4\pi M_s = 2267$ G and $\Delta H = 490$ Oe, the calculated maximum insertion loss is 20.3 dB at 4.11 GHz. The measured maximum of 23 dB occurs at 4.34 GHz. The bandwidth over which the insertion loss varies within 3 dB from the peak value was calculated to be 0.94 GHz, compared with the measured value of 0.75 GHz. The discrepancy between measured and calculated results may be attributed to the lack of accurate knowledge of the magnetization and line width at the surface and also to the approximation involved in neglecting the toroid's vertical sidewalls. The experimental and theoretical results of [21] show a 40% variation in the line width versus frequency. In Fig. 9, if the line width were 400 Oe instead of the measured value 490 Oe ($\simeq$ 18% lower), the calculated peak insertion loss would increase to 22.5 dB at 4.12 GHz with a bandwidth of 0.81 GHz. On the other hand, if the magnetization were 2400 G instead of 2267 G ($\simeq$ 6% higher), the peak loss would become 21.9 dB at 4.31 GHz and the bandwidth would decrease slightly to 0.93 GHz. The best agreement with measurement occurs when $4\pi M_s$ is taken to be 2400 G and ΔH is taken to be 400 Oe. This choice gave a peak attenuation of 24.2 dB at 4.32 GHz and a bandwidth of 0.8 GHz. It should be noted that the symmetric current solution gives worse agreement with measurements than the asymmetric current solution, as shown in Fig. 9. No reasonable perturbation in the magnetization ($>16\%$) was able to reduce the discrepancy between the symmetric current solution and the measurement. It should be possible to improve the model by measuring the ferrite properties at various in-band frequencies for the specified surface roughness and then using an interpolation process to determine the properties at other frequencies.

IV. Conclusion

The propagating mode of an infinitely long magnetostatic surface wave transducer was analyzed using a rigorous full-wave moment method analysis. Several multilayer structures were studied at frequencies in and just above the MSSW frequency band.

At frequencies in the MSSW band, the transducer mode has a complex propagation constant, reflecting the

fact that energy is lost to radiating MSSW's. No constraining assumption was made with regard to current symmetry across the width of the transducer and this was found to have a significant effect on the calculation of transducer mode attenuation at frequencies near the upper limit of the MSSW band. The real part of the propagation constant was found to be significantly different from the values calculated using the conventional approximation, which neglects the magnetic effects of the ferrite. This discrepancy will most affect calculations of the input reactance of finite length transducers.

The imaginary part of the microstrip propagation constant peaks at the upper end of the MSSW frequency band, but it can also peak again at higher frequencies. This occurs even though conventional MSSW's are not excited at these frequencies. The extra peak is associated with above-resonance magnetic surface waves, which themselves have complex (partially evanescent) propagation constants. This extra peaking behavior cannot be predicted if the line current is assumed symmetric.

Finally, measurements of the insertion loss of an experimental transducer were made using a ferrite toroid placed on a microstrip line. The measurements are in reasonable agreement with the theory.

The analysis presented in this paper can be extended in future work to include the coupling between two microstrip lines. Also, more extensive study of the complex mode surface waves is necessary to judge their potential and effect in practical transducers.

APPENDIX

The semispace Green's function G_1 in (8) is

$$\overline{\overline{G}}_1 = \frac{jY_c}{kk_d}\begin{bmatrix} \beta_y^2 - k_d^2 & -\beta_x\beta_y \\ -\beta_x\beta_y & \beta_x^2 - k_d^2 \end{bmatrix}$$

where

$$Y_c = \sqrt{\frac{\epsilon}{\mu_0}}$$

$$k_d = \omega\sqrt{\mu_0\epsilon}$$

$$k = \left(\beta_x^2 + \beta_y^2 - k_d^2\right)^{1/2}.$$

ACKNOWLEDGMENT

The authors gratefully acknowledge the Raytheon Company's Special Microwave Device Operation for providing the ferrite toroids used in the measurements. Also, Prof. N. E. Buris of the University of Massachusetts contributed the magnetostatic data and a number of helpful comments.

REFERENCES

[1] E. El-Sharawy and R. Jackson, "Coplanar waveguide and slot line on magnetic substrates: Analysis and experiment," *IEEE Trans. Microwave Theory Tech.*, vol. 36, pp. 1071–1079, June 1988.

[2] A. Ganguly and D. Webb, "Microstrip excitation of magnetostatic surface waves: Theory and experiment," *IEEE Trans. Microwave Theory Tech.*, vol. MTT-23, pp. 902–909, Dec. 1975.

[3] J. Sethares, "Magnetostatic surface wave transducers," *IEEE Trans. Microwave Theory Tech.*, vol. MTT-27, pp. 902–909, Nov. 1979.

[4] S. Bajpai, R. Carter, and J. Owens, "Insertion loss of magnetostatic surface wave delay lines," *IEEE Trans. Microwave Theory Tech.*, vol. 36, pp. 132–136, Jan. 1988.

[5] T. Gerson and J. Nadan, "Surface electromagnetic modes of a ferrite slab," *IEEE Trans. Microwave Theory Tech.*, vol. MTT-22, pp. 757–763, Aug. 1974.

[6] R. Rupin, "Electromagnetic modes of a ferromagnetic slab, *J. Appl. Phys.*, vol. 62, pp. 11–15, July 1987.

[7] N. Srivastava, "Surface wave propagation through a small gap between oppositely magnetized ferrite substrates," *IEEE Trans. Microwave Theory Tech.*, vol. MTT-26, pp. 213–215, Mar. 1978.

[8] A. Karsono and D. Tilley, "Retarded electromagnetic modes in ferromagnetic slab," *J. Phys. C: Solid State Phys.*, vol. 11, pp. 3487–3492, 1978.

[9] M. Marchand and A. Caille, "Asymmetrically guided magnetic polarizations in a ferromagnetic slab," *Solid State Commun.*, vol. 34, pp. 827–831, 1980.

[10] T. Itoh, "Spectral domain immittance approach for dispersion characteristics of generalized printed transmission line," *IEEE Trans. Microwave Theory Tech.*, vol. MTT-28, pp. 733–736, July 1980.

[11] M. Geshiro and T. Itoh, "Analysis of double-layered finlines containing a magnetized ferrite," *IEEE Trans. Microwave Theory Tech.*, vol. MTT-35, pp. 1377–1381, Dec. 1987.

[12] F. Lange, "Analysis of shielded strip and slot lines on a ferrite substrate transversely magnetized in the plane of the substrate," *Arch. Elek. Übertragung.*, Band 36, Heft 3, pp. 95–100, Mar. 1982.

[13] B. Lax and K. Button, *Microwave Ferrites and Ferromagnetics*. New York: McGraw-Hill, 1962.

[14] R. Damaon and J. Eshbash, "Magnetostatic modes of ferromagnet slab," *J. Phys. Chem. Solids*, vol. 19, pp. 308–320, 1961.

[15] W. Bongianni, "Magnetostatic propagation in a dielectric layered structure," *J. Appl. Phys.*, vol. 43, pp. 2541–2548, June 1972.

[16] J. Parekh and H. Bertoni, "Magnetostatic Rayleigh waves propagating along a tangential bias field on a YIG substrate," *J. Appl. Phys.*, vol. 45, pp. 434–445, Jan. 1974.

[17] R. Collin, *Field Theory of Guided Waves*. New York: McGraw-Hill, 1960.

[18] N. Das, Ph.D. thesis, University of Massachusetts, Amherst, MA, Sept. 1989.

[19] W. Huang and T. Itoh, "Complex modes in lossless shielded microstrip lines," *IEEE Trans. Microwave Theory Tech.*, vol. 36, pp. 163–165, Jan. 1988.

[20] W. Clark, "A technique for improving the figure-of-merits of a twin slab nonreciprocal phase shifter," *IEEE Trans. Microwave Theory Tech.*, vol. MTT-16, pp. 974–975, Nov. 1986.

[21] C. Buffler, "Effects of surface irregularities on single crystal resonance parameters," *J. Appl. Phys.*, vol. 31, May 1960.

[22] J. Adam, "Delay of magnetostatic surface waves in Y.I.G.," *Electron Lett.*, vol. 6, pp. 718–720, Oct. 1970.

[23] C. Buffler, "Ferromagnetic resonance near the upper limit of the spin wave manifold," *J. Appl. Phys.*, vol. 30, pp. 172S–175S, Apr. 1959.

El-Badawy El-Sharawy (S'85–M'89) was born on October 18, 1957, in Mansoura, Egypt. He received the B.Sc. and M.Sc. degrees (with honors) from Mansoura University, Egypt, in 1980 and 1984, respectively, and the Ph.D. degree from the University of Massachusetts, Amherst, in 1989, all in electrical engineering.

He joined Arizona State University in 1989, where he is currently an Assistant Professor of Electrical Engineering. His research interests center on the analysis and design of ferrite devices. Dr. El-Sharawy is a member of Eta Kappa Nu.

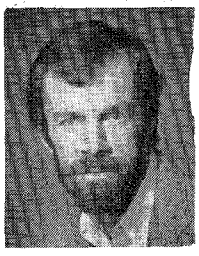

Robert W. Jackson (M'82–SM'88) was born in Boston, MA, in 1952. He received the B.S. (1975), M.S. (1979), and Ph.D. (1981) degrees in electrical engineering from Northeastern University, Boston, MA. His dissertation was concerned with nonlinear plasma interactions in the bow shock of the earth.

From 1981 to 1982, he was an Assistant Professor in the Department of Electrical Engineering at Northeastern University. Since 1982, he has been on the faculty of the Department of Electrical and Computer Engineering at the University of Massachusetts at Amherst, where he is currently an Associate Professor. His research interests include the electromagnetic aspects of integrated circuits, novel printed circuit and antenna structures, the modeling and design of planar ferrite devices, electromagnetics applied to nonlinear or anisotropic materials, and active microwave circuit design.